Earth and Environmental Science Transactions of the Royal Society of Edinburgh, **100**, 61–76, 2010 (for 2009)

Structural controls on melt segregation and migration related to the formation of the diapiric Schwerin Fold in the contact aureole of the Bushveld Complex, South Africa

Luke Longridge[1], Roger L. Gibson[1] and Paul A. M. Nex[1,2]

[1] School of Geosciences, University of the Witwatersrand, Johannesburg, PVT Bag 3, Wits, 2050, South Africa
Email: luke.longridge@wits.ac.za

[2] Umbono Group of Companies, Isle of Houghton, Johannesburg, South Africa

ABSTRACT: Partial melting of metapelitic rocks beneath the mafic–ultramafic Rustenburg Layered Suite of the Bushveld Complex in the vicinity of the periclinal Schwerin Fold resulted in a structurally controlled distribution of granitic leucosomes in the upper metamorphic aureole. In the core of the pericline, subvertical structures facilitated the rise of buoyant leucosome through the aureole towards the contact with the Bushveld Complex, with leucosomes accumulating in en-echelon tension gashes. In a subhorizontal syn-metamorphic shear zone to the southeast of the pericline, leucosomes accumulated in subhorizontal dilational structural sites. The kinematics of this shear zone are consistent with slumping of material off the southeastern limb of the rising Schwerin pericline. The syndeformational timing of leucosome emplacement supports a syn-intrusive, density-driven origin for the Schwerin Fold. Modelling of the cooling of the Rustenburg Layered Suite and heating of the floor rocks using a multiple intrusion model indicates that temperatures above the solidus were maintained for >600,000 years up to 300 m from the contact, in agreement with rheological modelling of floor-rock diapirs that indicate growth rates on the order of 8 mm/year for the Schwerin Fold.

KEY WORDS: diapiric fold, granite leucosomes, thermal modelling

The role of deformation in the initial segregation, migration and accumulation of leucosomes has been investigated in a wide variety of regional metamorphic terrains (e.g. Brown 1994 and references therein; Brown & Solar 1998; Kisters *et al.* 1998). Additionally, studies have demonstrated the weakening effect of melt on the rheology of rocks (e.g. Bai *et al.* 1997; Gleason *et al.* 1999; Holyoke & Rushmer 2002). Although many studies exist that demonstrate the relationship between deformation and melting in an orogenic context, few studies exist where melting and deformation relationships have been examined in contact metamorphic aureoles (e.g. Rosenberg & Berger 2000; Vernon *et al.* 2003). In the northeastern parts of the contact aureole to the Bushveld Complex, South Africa, a number of kilometre-scale periclinal fold structures are found in the upper amphibolite- to granulite-grade floor rocks underlying the Bushveld Complex. The Schwerin Fold is one of these periclinal structures developed in migmatitic rocks of the upper Transvaal Supergroup. Here, the interplay of deformation and anatexis and, particularly, the positive feedback loop between deformation-enhanced melt accumulation and migration, and the rheological consequences of deformation in partially molten rocks, can be investigated.

1. Melting sites and melt migration in metamorphic terranes

The importance of deformation in the migration and ascent of granitic magmas in orogens has been noted repeatedly (e.g. Brown 1994, 2005; Kisters *et al.* 1998) and, although the buoyancy of low-density granitic magma is a primary driving force for the ascent of the magma, fault systems and shear zones are needed as conduits. In addition to gravity-driven ascent of buoyant magma, non-hydrostatic stresses and pressure gradients may also drive melt into, and along structures. Strain localisation in migmatite terrains is a key factor in the accumulation, segregation and transport of granitic melt, and a positive feedback exists between deformation-initiated melt mobilisation, melt accumulation promoting ductile deformation processes and enhancing bulk strain partitioning, and the buoyant rise of segregated melts (Kisters *et al.* 1998). In orogenic terrains, where heating of rocks to upper amphibolite to granulite facies conditions is generally accompanied by progressive deformation, this deformation can result in the formation of low-pressure sites where melt can preferentially accumulate. These low-pressure sites can include boudin necks (Vernon *et al.* 2003), extensional shear bands (Brown *et al.* 1995), shear zones (Bhadra *et al.* 2007), and fold axial planes (Hand & Dirks 1992). These low-pressure sites also play a key role in the segregation of mafic selvedges from leucosome (Sawyer 1991). This melt accumulation leads to a localised increase in the ductility of the rocks in the vicinity of the melt, which in turn increases strain partitioning in the vicinity of the melt.

2. Regional geological setting and previous work

The intrusion of the ~8 km-thick, 2·06 Ga (Walraven *et al.* 1990) sill-like mafic-ultramafic Rustenburg Layered Suite (RLS) of the Bushveld Complex (Fig. 1) into the sedimentary

 doi:10·1017/S1755691009016119

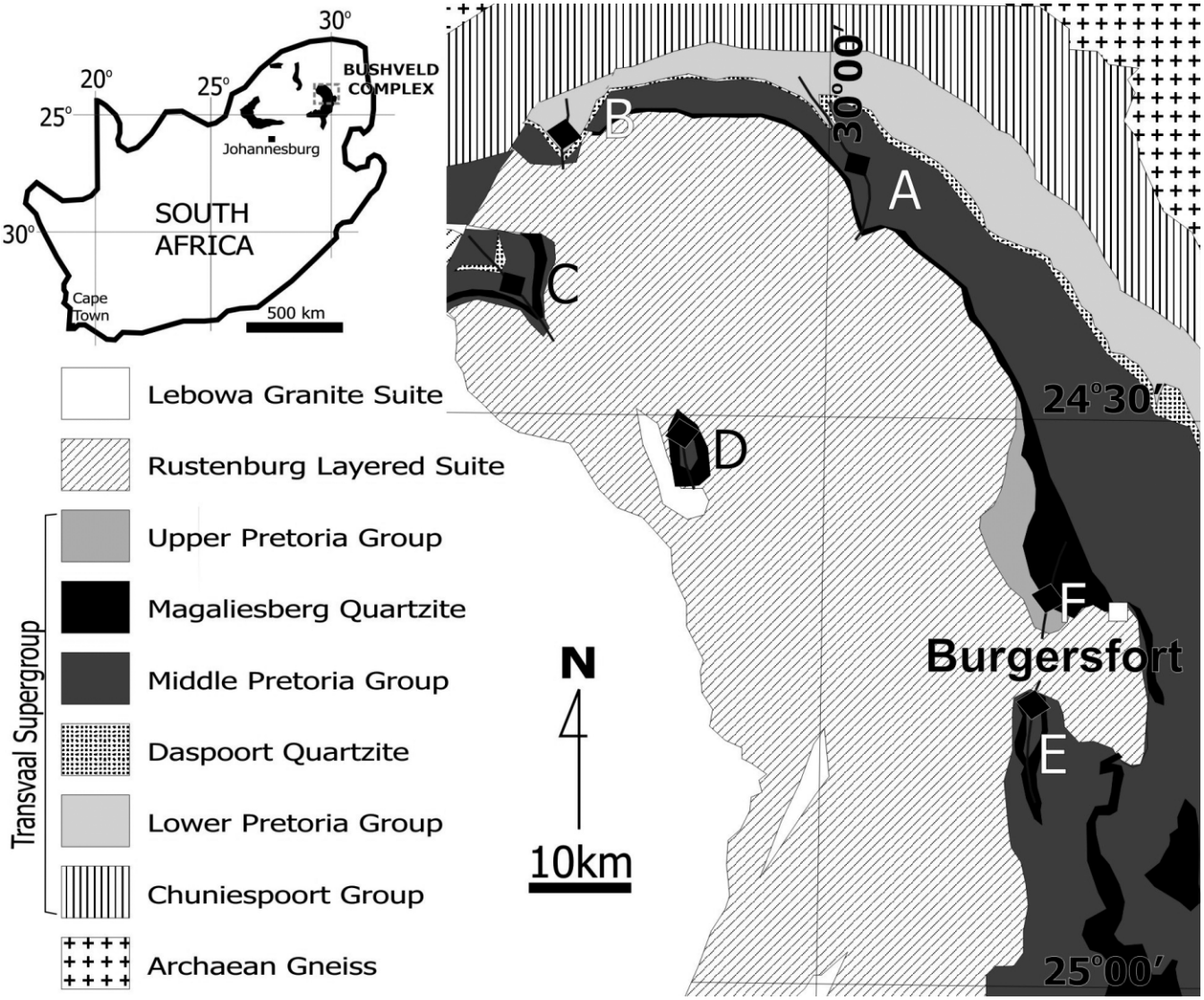

Figure 1 Geological map of the northeastern limb of the Bushveld Complex, showing locations of the Schwerin Fold (A) and other fold structures: B=Katkloof; C=Phosiri; D=Phepane; E=Steelpoort; F=Derde Gelid. After 1:250 000 Geological Series sheets 2429B (Chuniespoort) and 2430A (Wolkberg) (Schwellnus *et al.* 1962).

rocks of the Transvaal Supergroup formed a metamorphic aureole in the floor rocks that extends up to tens of kilometres from the RLS contact. Since the RLS intruded horizontally, the term 'upper aureole' is used to describe the highest-grade rocks that lie immediately below the contact with the RLS. In the upper aureole, metamorphic grade reached granulite grade (indicated by the presence of metamorphic orthopyroxene locally in rocks proximal to the RLS contact; Uken 1998; Johnson *et al.* 2003), and migmatites formed in pelitic and psammitic rocks. Mapping of the floor rocks to the RLS in the northeastern Bushveld Complex has revealed a number of domes and periclines within both these high-grade migmatites and the lower-grade unmigmatised metapelites (Fig. 1). Early workers suggested that these structures formed as a result of regional compression and modification of pre-Bushveld folds during the intrusion of the RLS (Sharpe & Chadwick 1982; du Plessis and Walraven 1990; Hartzer 1995), but more recent work (Uken & Watkeys 1997; Uken 1998; Johnson *et al.* 2004) has suggested that these structures are the result of gravity-induced diapiric rise of low-density argillaceous, arenaceous and calcareous rocks into the dense mafic magmas of the RLS (Uken & Watkeys 1997), a mechanism initially proposed by Button (1978). The Schwerin Fold (located ~60 km NNW of the town of Burgersfort; Fig. 1) is one such pericline and is developed in rocks of the upper Pretoria Group (Transvaal Supergroup; Fig. 2).

Contact metamorphic effects beneath the RLS in the northeastern Bushveld Complex extend throughout the Pretoria Group, with temperatures of ~450°C in rocks of the lower Pretoria Group (Waters & Lovegrove 2002), and up to ~750°C near the contact with the RLS (Johnson *et al.* 2003, 2004). Bulk compositional variation, as well as metamorphic grade, controls mineral assemblages in the aureole. A regional study of anatectic migmatites in the eastern Bushveld Complex aureole by Johnson *et al.* (2003) emphasised the role of deformation in the migration and ascent of melts. They noted that, throughout the upper aureole, migmatites occur in rocks that are gently folded on a m-scale, with a moderate to weak foliation, and that are locally more intensely strained (particularly in the vicinity of the km-scale periclines). In the zone closest to the contact with the RLS, Johnson *et al.* (2003) described migmatites associated with a variety of structural features. These include quartz-sillimanite veins, approximately parallel to the subhorizontal bedding in the area, which are folded into cm- to dm-scale open to tight, locally ptygmatic folds, and which contain a foliation similar to that in the host

https://doi.org/10.1017/S1755691009016119 Published online by Cambridge University Press

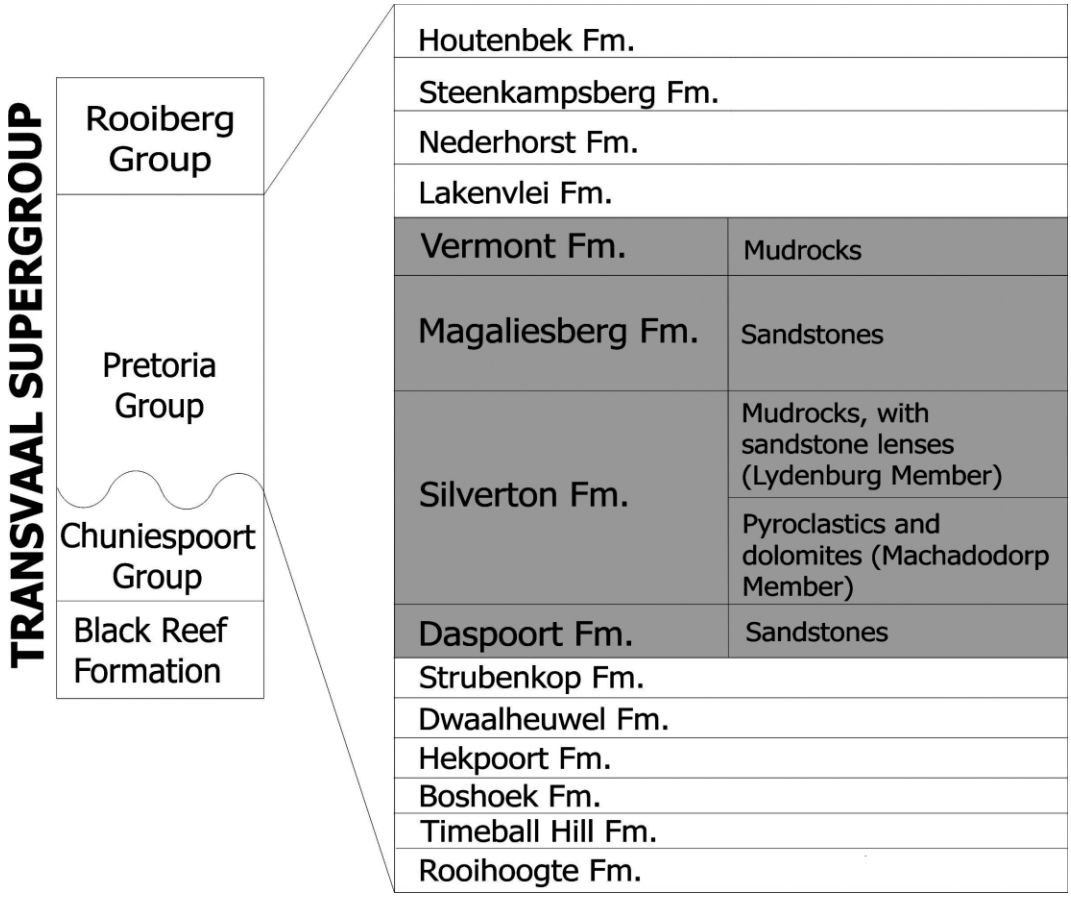

Figure 2 Stratigraphy of the Transvaal Supergroup showing the detailed stratigraphy and lithologies of the Pretoria Group in the study area. Formations which dominate the study area are shaded in grey. Modified after Eriksson *et al*. (1993).

rocks. They interpreted these features as channels for H_2O- and volatile-rich melts. Also noted were higher-strain domains commonly associated with discordant leucosomes, that are commonly located above the small antiformal closures of folded quartz-sillimanite veins. The significance of this contemporaneous relationship between melting and deformation is explored further below.

3. Geology of the Schwerin Fold

The Schwerin Fold (Figs 1, 3) is a kilometre-scale, upright to steeply inclined, gently- to moderately-plunging periclinal structure that is developed in the arenaceous to argillaceous rocks (with minor pyroclastic and calcareous rocks) of the Pretoria Group (uppermost Transvaal Supergroup; Fig. 2). The contact with the RLS is at the level of the Vermont Formation. The Schwerin Fold has a maximum wavelength of ~8 km and an amplitude of ~5 km, but is disharmonic, and the interlimb angle decreases to that of a tight fold in the stratigraphically-highest layers closest to the RLS. The fold is asymmetric, with steeper dips (70–80°) on the western limb and shallower dips (20–40°) on the eastern limb (Fig. 3). The regional dip of the rocks in the area is towards the RLS (~25°SW), subparallel to the magmatic layering in the RLS. The Schwerin Fold differs from other periclines in the floor to the RLS in its asymmetry, and in that it has a curved axial trace, which is perpendicular to the contact with the RLS at the contact but curves to subparallel to the RLS strike away from the contact. However, like the other periclines in the RLS aureole (Uken & Watkeys 1997; Uken 1998), it has gentle to open synclinal areas adjacent to both limbs. For simplicity of structural analysis, the Schwerin Fold has been divided into three sub-domains.

3.1. Domain 1 – metasediments in the contact aureole away from the Schwerin Fold

At a distance of 3–6 km from the contact with the RLS, in the NE of the study area, pelitic rocks of the Lydenburg Member (Silverton Formation; Fig. 2) dip shallowly (~25°) SW. The rocks retain original sedimentary compositional layering, defined by layers which are more or less biotite-rich (Fig. 4A). A moderately SE-dipping (~35°), moderate to weak foliation defined by biotite occurs oblique to bedding (Fig. 4B). The rocks are not migmatised and contain the assemblage andalusite–biotite–cordierite–quartz–ilmenite/magnetite. The matrix consists of fine (0·01–0·2 mm) quartz, biotite and ilmenite/magnetite. Andalusite porphyroblasts are generally stubby to elongate, 1–5 cm long, chiastolitic, and lie with their longest dimensions within the bedding plane (indicating a compositional control). Andalusite contains graphite and small (0·05–0·1 mm) muscovite and quartz inclusions towards the core, and larger (0·1–0·2 mm) quartz and biotite inclusions near the rim. Cordierite porphyroblasts are 0·5–5 mm in size, and some cordierite porphyroblasts are texturally zoned, with an inclusion-rich core and an inclusion-free rim. Cordierite contains fine (0·01–0·1mm) inclusions of quartz, biotite and ilmenite/magnetite, which are aligned parallel to the foliation observed in the matrix. Andalusite has inclusions aligned parallel to the foliation, although this is less distinctive owing to the generally inclusion-free nature of andalusite relative to cordierite. No pressure shadows exist adjacent to either andalusite or cordierite (which, together with alignment of inclusions, supports post-tectonic growth). This contrasts with

https://doi.org/10.1017/S1755691009016119 Published online by Cambridge University Press

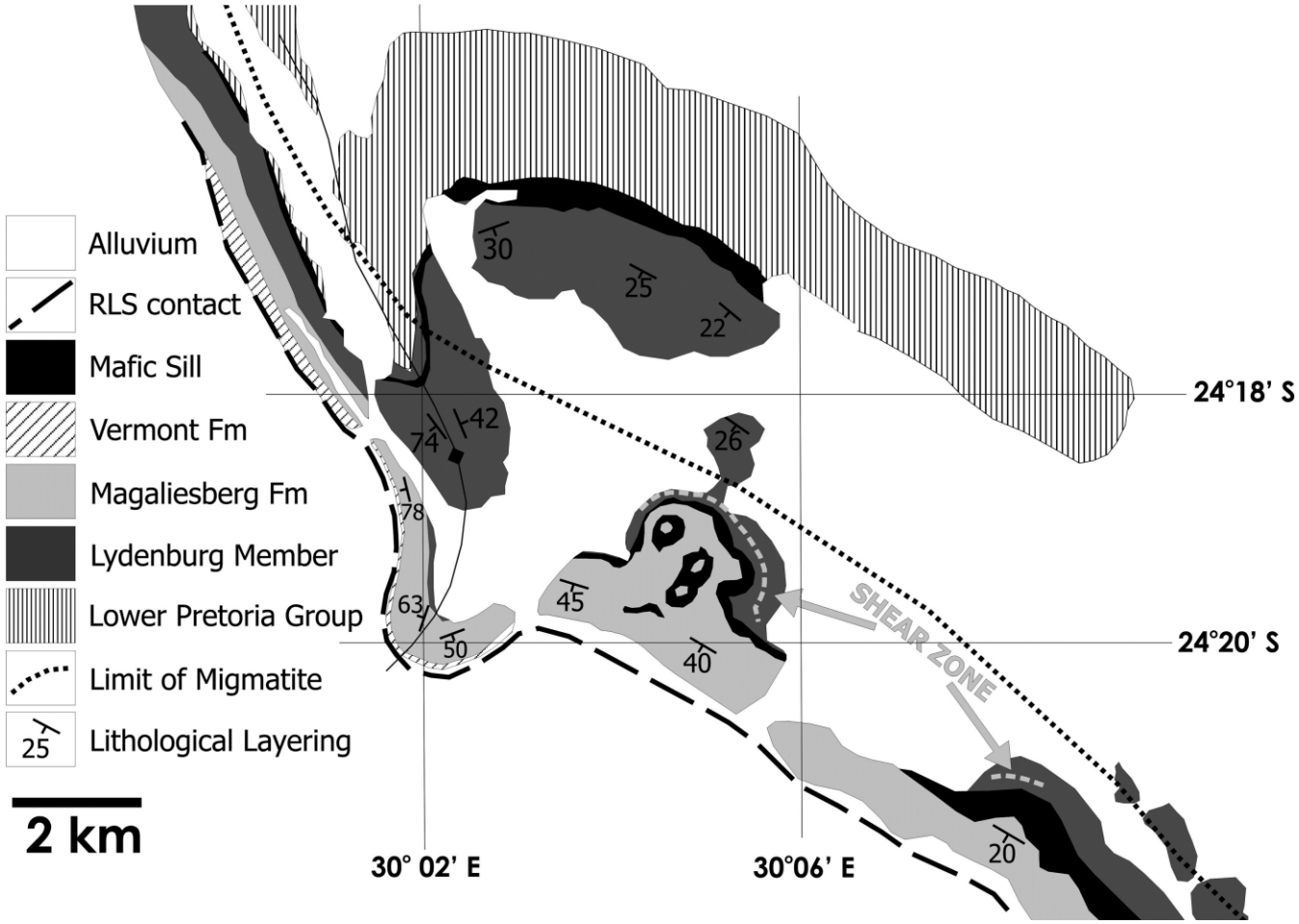

Figure 3 Geological map of the Schwerin Fold, showing the lower limit of migmatite development in the contact aureole. Note the change in strike of the axial surface and the steeper dip of strata on the western limb. Modified after Uken (1998).

textures further from the RLS contact reported by Uken (1998), which show flattening of the bedding-parallel foliation around andalusite porphyroblasts.

3.2. Domain 2 – metasediments from the Schwerin Fold

The second domain includes metapelites (Lydenburg Member) in the core of the Schwerin Fold, as well as the quartzites (Magaliesberg Formation) closer to the contact with the RLS (Fig. 3). Closest to the contact with the RLS, the Magaliesberg Formation quartzite forms a prominent ridge. This quartzite describes a moderately SW-plunging anticlinal fold with a 3 km wavelength. Bedding dip varies from ~70°WSW to vertical on the western limb of the fold to ~40°S to SSE on the southeastern limb of the fold. The quartzites are well bedded, and retain numerous original sedimentary features, including trough cross-bedding and ripple marks. Cross-bedding confirms that the rocks have not been overturned. The rocks are coarsely recrystallised and 2–3 cm long euhedral quartz crystals are found filling vugs in the quartzite, consistent with hydrothermal fluid activity. In places on the western limb a weak foliation is defined by elongate quartz grains. This foliation is slightly oblique to bedding, striking 010° and dipping steeply at 70°W. Gentle to open folds, with a 2–5 m wavelength and 0·5 m to 1 m amplitude are present in the quartzites, and plunge steeply NW.

The core of the Schwerin Fold is defined by a ridge of pelitic to semi-pelitic rocks of the Lydenburg Member (Figs 2, 3) and calc-silicates and volcanic breccias of the Machadodorp Member (Fig. 2). Bedding is defined by mm- to cm-thick siliceous layers and sedimentary structures (graded, flaser and rare trough cross-bedding) that indicate a right-way-up sequence. Bedding is generally moderately dipping, but has a variable orientation caused by dm- to m-scale open to tight folds. A penetrative subvertical foliation is present which, at distances of >2 km from the contact with the RLS, is defined by biotite.

The northeastern parts of Domain 2 straddle the lower limit of migmatite development, and contain the assemblage andalusite–biotite–cordierite–plagioclase–muscovite–quartz in lower-grade metapelites, and andalusite–biotite–cordierite–plagioclase–muscovite–fibrolite–quartz in higher-grade samples. Biotite occurs as 0·5–1 mm grains with 0·02–0·1 mm inclusions of quartz, although it is generally inclusion-free. It is locally retrogressed to chlorite. Texturally-late muscovite is present as large (>1 mm) vermicular grains, which overgrow the foliation. Cordierite is 0·5–1 mm in size, and contains fine (0·01 mm) inclusions of quartz and coarser (0·1 mm) inclusions of biotite (Fig. 4H). It is commonly texturally zoned, with inclusion-free rims surrounding inclusion-rich cores, and may show sector twinning. Cordierite porphyroblasts are commonly lensoid and aligned with the foliation (indicating syntectonic growth). In higher-grade samples, fibrolite is developed around biotite, and appears to form at the expense of biotite (Fig. 4G). Where fibrolite is developed, it is not distributed throughout the sample, but occurs as discrete 'seams' within the sample, along which it replaces biotite. Locally, 1–3 cm-long andalusite porphyroblasts are aligned parallel to the biotite and fibrolite foliations, supporting

https://doi.org/10.1017/S1755691009016119 Published online by Cambridge University Press

syn-tectonic growth, although textural evidence indicates that fibrolite postdates andalusite.

A thin garnet-bearing horizon below the migmatite zone contains the assemblage garnet–biotite–cordierite–muscovite–ilmenite–quartz, with 0·2–1 mm subhedral garnet porphyroblasts preferentially developed in ilmenite-rich beds. Garnet contains 0·01–0·02 mm inclusions of quartz and ilmenite, and the moderate biotite foliation may bend gently around the garnet porphyroblasts, although generally it does not wrap around garnet, suggesting late- to post-tectonic growth of the latter.

Within ~2 km of the outcrop of the RLS contact, the pelitic rocks are cut by coarse-grained to pegmatitic quartz–feldspar–fibrolite–tourmaline–muscovite leucosomes, which may contain peritectic cordierite (see also Johnson *et al.* 2003). As the contact is approached, a progressive increase in the volume of leucosome is seen. In the lowermost migmatite zone, the leucosomes develop within metapelites adjacent to quartz-sillimanite veins (originally more psammitic beds; Johnson *et al.* 2003) as 1–5 cm long, 0·5–2 cm wide veins (Fig. 4D) but, with decreasing distance from the contact, they develop into tension gashes up to 30 cm in length and ~5 cm wide (Fig. 4E). As the volume of leucosome increases, the leucosomes become more pod-like, and cross-cut the pelite bedding, forming an interconnected network (Fig. 4F). The leucosomes are coarsely crystalline (quartz grains ~5 mm) to pegmatoidal (quartz grains ~20 mm). Leucosomes with the finest grain size retain a relict fibrolite foliation within them, with a similar orientation to that observed in the pelites, but this foliation is absent in the coarser pegmatites. Granophyric textures are observed; these commonly overgrow fibrolite aggregates, which also occur as inclusions in quartz. Although the leucosomes appear in structurally controlled sites, there is no evidence that deformation continued following leucosome crystallisation. Minerals within the leucosomes are unstrained, and leucosomes show no penetrative fabric.

The modal proportion of fibrolite increases in tandem with the volume of leucosome towards the RLS contact. Textural evidence suggests that fibrolite development was at the expense of biotite, rather than andalusite, and that fibrolite-rich seams correspond to pathways recording the passage of an H_2O-rich volatile phase, which may have been responsible for the fluid-fluxed incongruent melting of biotite (Johnson *et al.* 2003). Johnson *et al.* (2003) suggested that the reaction Pl+Bt+Qtz=Kfs+Crd+L is the most likely melt-producing reaction for typical Lydenburg Member metapelite compositions, although melt-producing reactions vary with temperature and X_{Mg}, and an influx of H_2O may have generated the congruent melting reaction Kfs+Pl+Bt+Crd+Qtz+H_2O=L.

A mafic sill is found at the base of the Lydenburg Member in both the migmatites and lower grade rocks and (like the stratigraphy) is cut by the isograds in the aureole (Fig. 3). This sill has no obvious chill margin, but field evidence (textural and mineralogical variation) suggests that it may be a composite sill composed of at least two phases. It is metamorphosed, with an assemblage tremolite–actinolite–plagioclase–quartz indicating significant rehydration, and does not preserve any original igneous textures.

3.3. Domain 3 – migmatitic shear zone east of the Schwerin Fold

Domain 3 is found in the southeastern part of the study area, on the southeastern limb of the syncline flanking the Schwerin Fold (Fig. 3). Here the uppermost rocks (Silverton Formation) contain a 50 m to 100 m-wide subhorizontal to gently SW-dipping bedding-parallel shear zone (Fig. 3). Below the shear zone, metapelites preserve compositional banding as alternating biotite-rich and quartz-feldspar-rich layers, or as staurolite-rich layers. In less competent lithologies in the shear zone, bedding appears transposed, with rootless tight to isoclinal cm-scale folds of either quartz–feldspar or biotite-rich layers, indicating remnant bedding (Fig. 5A).

Assemblages in more biotite-rich layers are generally quartz–biotite–plagioclase feldspar, with some perthitic K-feldspar, cordierite and muscovite. Generally the rock consists of fine (0·02–0·1 mm) quartz, plagioclase and biotite with a strong foliation, and 0·5–1 mm vermicular muscovite overgrowing the foliation. Cordierite is 0·5–1 mm in size, and contains 0·01 mm inclusions of biotite and quartz. Andalusite is rare, and no fibrolite is developed in these rocks. A shallow WNW-dipping foliation, defined by biotite, wraps around low strain lenses that contain a relict foliation with an obliquity of 15° to 70° relative to the main foliation (Fig. 5B). Pressure shadows around these low strain lenses contain slightly coarser (0·2–0·4 mm) quartz and feldspar (Fig. 5B). No change in assemblage is observed between these low strain lenses and the foliated matrix.

The shear zone is characterised by open, tight and isoclinal m-scale folding (Fig. 5A, C), with fold vergence typically towards the S, SW or W, and an axial planar foliation, defined by biotite, which typically dips shallowly WNW (Fig. 5C). Locally, mullions are present in fold hinges. Listric extensional shear bands (ESBs) are widespread, and are filled with coarse to pegmatoidal quartz–feldspar–tourmaline–muscovite leucosomes, containing 0·5–5 cm biotite schlieren. ESBs range in size from a few cm long and a few mm wide to metres in length and >10 cm wide. Boudins are found rarely in the more competent psammitic layers, and are generally symmetrical, with only weak local asymmetry, indicating an approximately top-to-the-SE sense of shear.

Folds vary from cm-scale recumbent isoclinal folds to gently inclined open m-scale folds, to upright ptygmatic m-scale folds, although most folds are ~0·5 m to 1 m in wavelength, and are tight to isoclinal, gently plunging, and moderately to gently inclined (Fig. 5C). Although there is a large variation in fold hinge azimuth, no sheath folds were found. The foliation is refracted by compositional layering. Deformation styles vary within the shear zone, depending upon the lithology. In pelitic rocks, which are the predominant lithology towards the base of the shear zone, the rocks are highly foliated. In this zone of less competent lithologies, folds are rare and, where seen, are cm-scale and isoclinal (Fig. 5A), consistent with extreme transposition. Towards the top of the shear zone, a more competent psammitic lithology predominates, and larger-scale folds, ESBs and boudins are common. Below the shear zone, where only minor leucosome veins are found in boudin necks, the rocks lack evidence of shear-related deformation. The shear zone can be traced over a strike length of ~10 km southeastwards from the hinge of the Schwerin Fold; however it has not been found near the hinge or on the northern limb of the Schwerin Fold.

Leucosomes from ESBs within the shear zone have an assemblage comprising quartz–microcline–biotite–muscovite–plagioclase–tourmaline ± cordierite. Microcline is extremely coarse (>5 mm) and contains ~0·2 mm rounded to subidioblastic inclusions of quartz, plagioclase, muscovite and biotite (Fig. 5F). Biotite occurs either as small (~0·5 mm) euhedral flakes or as larger (~3 mm) schlieren, which are unlikely to be crystallisation products, but appear to have been entrained during anatexis and leucosome movement (see Fig. 5E). This biotite is slightly more magnesian (Mg#=50–53) than that from the host rocks (Mg#=33–39; Longridge 2006), and may be the restitic product of the partial melting which formed the leucosomes. Muscovite is commonly poikilitic. Leucosomes

https://doi.org/10.1017/S1755691009016119 Published online by Cambridge University Press

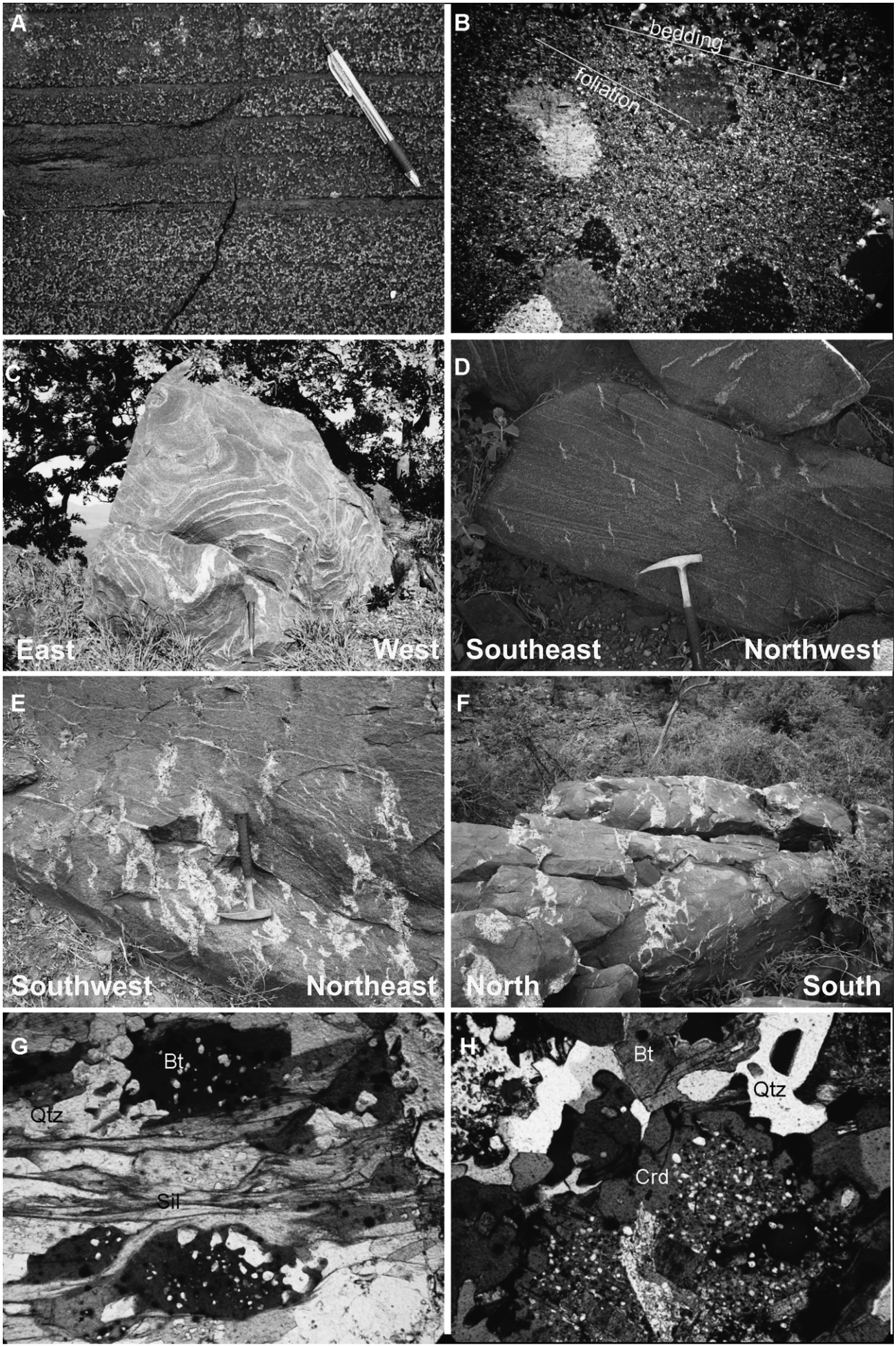

https://doi.org/10.1017/S1755691009016119 Published online by Cambridge University Press

may contain biotite selvedges at their margins. These leucosomes are similar to the small granite sheets found in the migmatite zone in the eastern Bushveld Complex metamorphic aureole, which Harris *et al*. (2003) attributed to incongruent melting of biotite in the pelites of the Silverton Formation. No post-crystallisation deformation features or any evidence for strain is observed in the leucosomes, indicating that deformation had ceased in the shear zone by the time the leucosomes had crystallised.

4. Structural geology of the Schwerin Fold

The broad structure of the Schwerin Fold differs from other comparable structures such as the Katkloof Fold (Fig. 1), in that it has a strongly curved axial trace. At the contact with the RLS, the Schwerin Fold hinge plunges towards the SW, whereas the fold hinge in the core of the fold has a SSE plunge (Fig. 6). Both the eastern and western limbs of the Schwerin Fold give way to open synclines, where the strike of the rocks adjacent to the pericline gently curves into the regional NW–SE strike of the Pretoria Group rocks.

A structural investigation by Uken (1998) focused primarily on the non-migmatitic core of the Schwerin Fold, where he noted boudinaged calc–silicate layers and cuspate–lobate folds with radially oriented fold axes. These folds were noted to have an associated axial planar cleavage, and slickenside lineations on bedding surfaces, consistent with a flexural slip fold mechanism (Uken 1998). Also noted was a non-penetrative bedding-parallel S_2 cleavage in the limbs of the fold.

4.1. Low-grade metapelites away from the Schwerin Fold

In the northeast of the study area, low-grade metapelites are not affected by the Schwerin Fold, and structures are more representative of the regional trends in the floor rocks to the RLS. In this area, the bedding in metapelites of the Lydenburg Member dips moderately towards the RLS (average orientation 124°/18°SW) and the oblique foliation defined by biotite has an average orientation of 232°/32°SE (Fig. 6B[II]).

4.2. Quartzites adjacent to the RLS contact

Adjacent to the RLS contact, competent Magaliesberg Formation quartzites appear to inhibit foliation formation, with the foliation only locally developed and defined by an elongation of quartz grains. Bedding orientations in the hinge of the fold define a π-pole girdle, which gives a fold axis plunge of 47° on an azimuth of 227° (Fig. 6D[II]). Bedding data from the northwestern limb are more scattered than those from the southeastern limb. A best-fit partial π-pole girdle through these data defines a fold plunge of 52° on 346° (Fig. 6D[II]). A progressive change in bedding orientation occurs from ~170°/78°W in the north to ~195°/62°W in the south. Bedding orientations on the northwestern limb are steeper than those on the southeastern limb.

4.3. Metasediments from the core of the Schwerin Fold

In the core of the Schwerin Fold, bedding data from the Lydenburg Shale Member show more scatter than data from the quartzites adjacent to the contact. The data define a π-pole girdle with a fold axis plunge of 26° on 188° (Fig. 6A[II]). This is slightly shallower than the hinge-line orientations of m-scale outcrop folds, but the azimuths nonetheless correspond well. Foliations from metapelites of the Lydenburg Member are approximately vertical to steeply W-dipping and N–S trending in the centre of the pericline, but some variation in orientation occurs.

4.4. Shear Zone

Within and adjacent to the shear zone to the east of the Schwerin Fold, a number of structural elements are present. Bedding and foliation orientations are variable, but, on average, they are 146°/16°SW and 202°/20°W, respectively (Fig. 6C[II]).

Extensional shear band (ESB) orientations are also variable, owing to their listric nature, and give an average orientation of 106°/22°S (Fig. 6C[II]; given the curved character of the ESBs, an average value is likely to be the best representation of their orientation). ESBs are not present as a conjugate set, but display a consistent vergence towards the SSW. Boudin axes plunge shallowly to the east or west. Lineations are also sub-horizontal, and plunge either shallowly NNW or SSE, with the exception of a single outlier, which has an orientation of 30° on 225°. Most lineations are located on bedding surfaces, and are mineral stretching lineations. Fold hinges have highly variable orientations. The plunge of most folds is quite shallow, but azimuths vary from N to W and S.

5. Structural interpretation of the Schwerin Fold

In order to understand the orientation of structures in the Schwerin Fold, consideration must be given to the orientation of rocks in the adjacent RLS. A recent re-evaluation of the palaeomagnetism of the Bushveld Complex (Letts 2007), indicates that the RLS acquired its remnant magnetisation (i.e. passed through the Curie temperature) whilst still horizontal. If the fold and shear zone formed before this (see below; also Uken & Watkeys 1997; Uken 1998), then their geometry can only be determined by back-rotating them by an amount equivalent to the average dip of the RLS. Thus, by removing the effects of the regional ~20°SW dip of the RLS and its floor rocks, one can obtain the 'original' orientation of the Schwerin Fold.

Figure 4 (A) Hornfels from the lower aureole (below the migmatite zone) showing lithological layering defined by variable biotite content. Spots are chiastolite porphyroblasts. (B) Photomicrograph of (A) showing cordierite and andalusite porphyroblasts, and a weak foliation slightly oblique to bedding (crossed polars; width of field of view=4 mm). (C) Folding of migmatitic metapelites in the core of the Schwerin Fold. Note the subvertical orientation of the axial plane to the folds, which mirrors the large-scale structure of the pericline. (D) En-echelon tension gashes oriented oblique to bedding in metapelite from the core of the pericline, in the lower migmatite zone. (E) Enlargement of tension gashes in rocks closer to the contact with the RLS than (D), on the western limb of the fold. (F) Patchy leucosome network no longer restricted to tension gashes (upper migmatite zone). (G) Photomicrograph of metapelite from the pericline core, showing fibrolite seams developed at the expense of biotite (uncrossed polars, width of field of view 2 mm). (H) Photomicrograph of metapelite from the core of the pericline, showing a large cordierite porphyroblast with an inclusion-rich core and clear rim, in addition to biotite and corroded quartz, indicating melting (crossed polars; width of field of view=2 mm). Mineral abbreviations after Kretz (1983).

https://doi.org/10.1017/S1755691009016119 Published online by Cambridge University Press

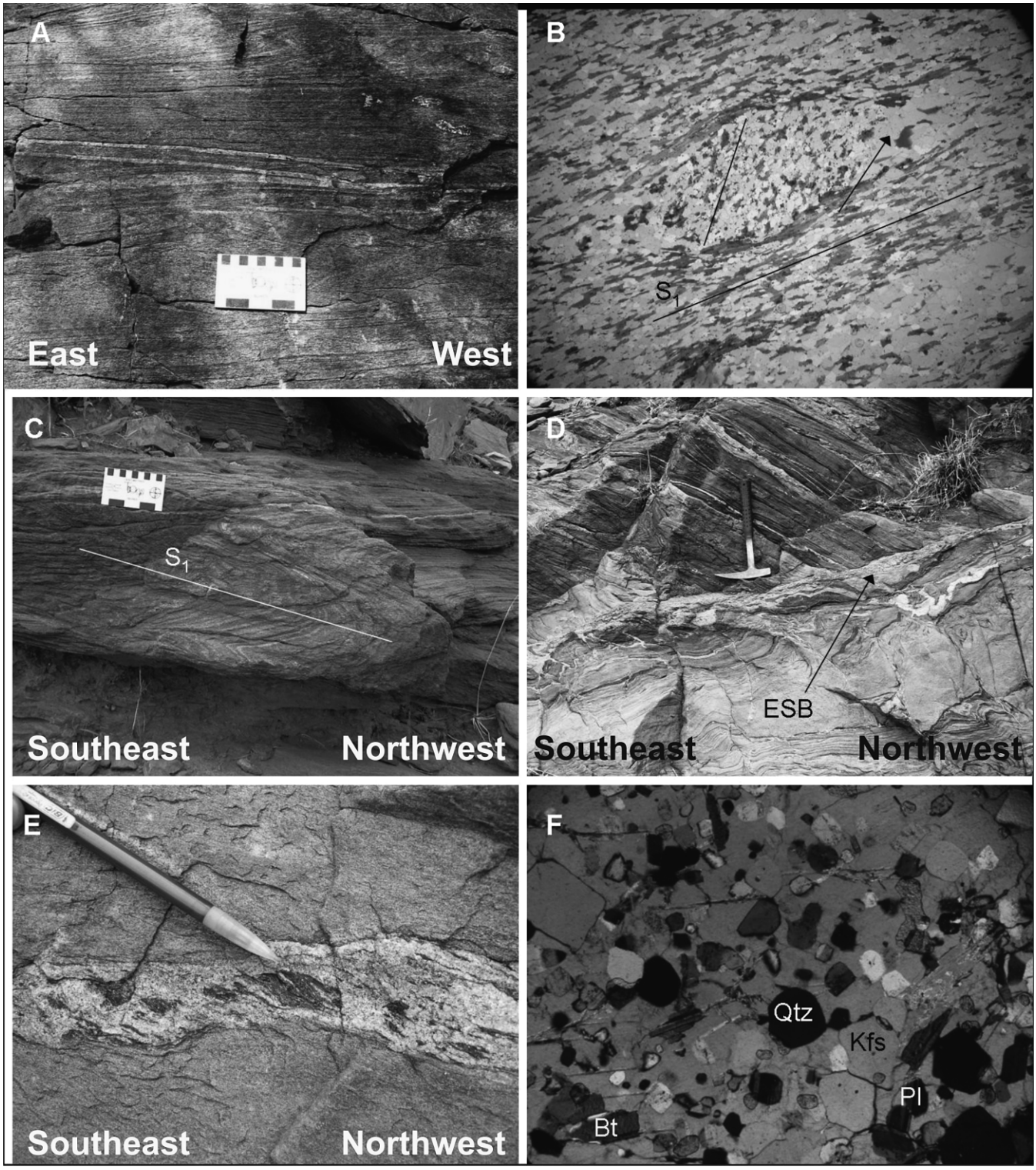

Figure 5 Outcrop and microscopic structural characteristics of the shear zone: (A) Isoclinal intrafolial folds and transposed bedding in semi-pelitic schist; (B) Oblique earlier foliation in a low-strain lens within quartz-biotite schist. Note coarse quartz grains in the pressure shadow formed by this lens. This texture is interpreted as a composite foliation due to progressive shearing deformation rather than overprinting deformation events (uncrossed polars, width of field of view = 5 mm); (C) Tight SE-verging folds with a shallow NE-dipping axial planar foliation; (D) Shallow SE-verging extensional shear bands filled with granitic leucosome; (E) Close-up view of a leucosome within an extensional shear band, containing biotite schlieren which indicate vergence towards the southeast; (F) Photomicrograph of a granitic leucosome, showing a large (~5mm) K-feldspar with euhedral to subhedral quartz, plagioclase and biotite inclusions, indicating crystallisation from a melt (crossed polars; width of field of view = 2 mm). Mineral abbreviations after Kretz (1983).

5.1. Low grade metapelites away from the Schwerin Fold

Metapelites in the contact aureole distal to the Schwerin Fold contain a penetrative subhorizontal cleavage that is typical of the RLS aureole away from periclinal structures (Uken 1998). This fabric is generally subparallel to bedding, but becomes axial planar to periclinal structures towards the core of these structures, creating a distinctive upward-closing fan pattern (Uken & Watkeys 1997; Fig. 9).

Rotation of the structural data through rotation by 20° around a horizontal axis trending 135° results in an

https://doi.org/10.1017/S1755691009016119 Published online by Cambridge University Press

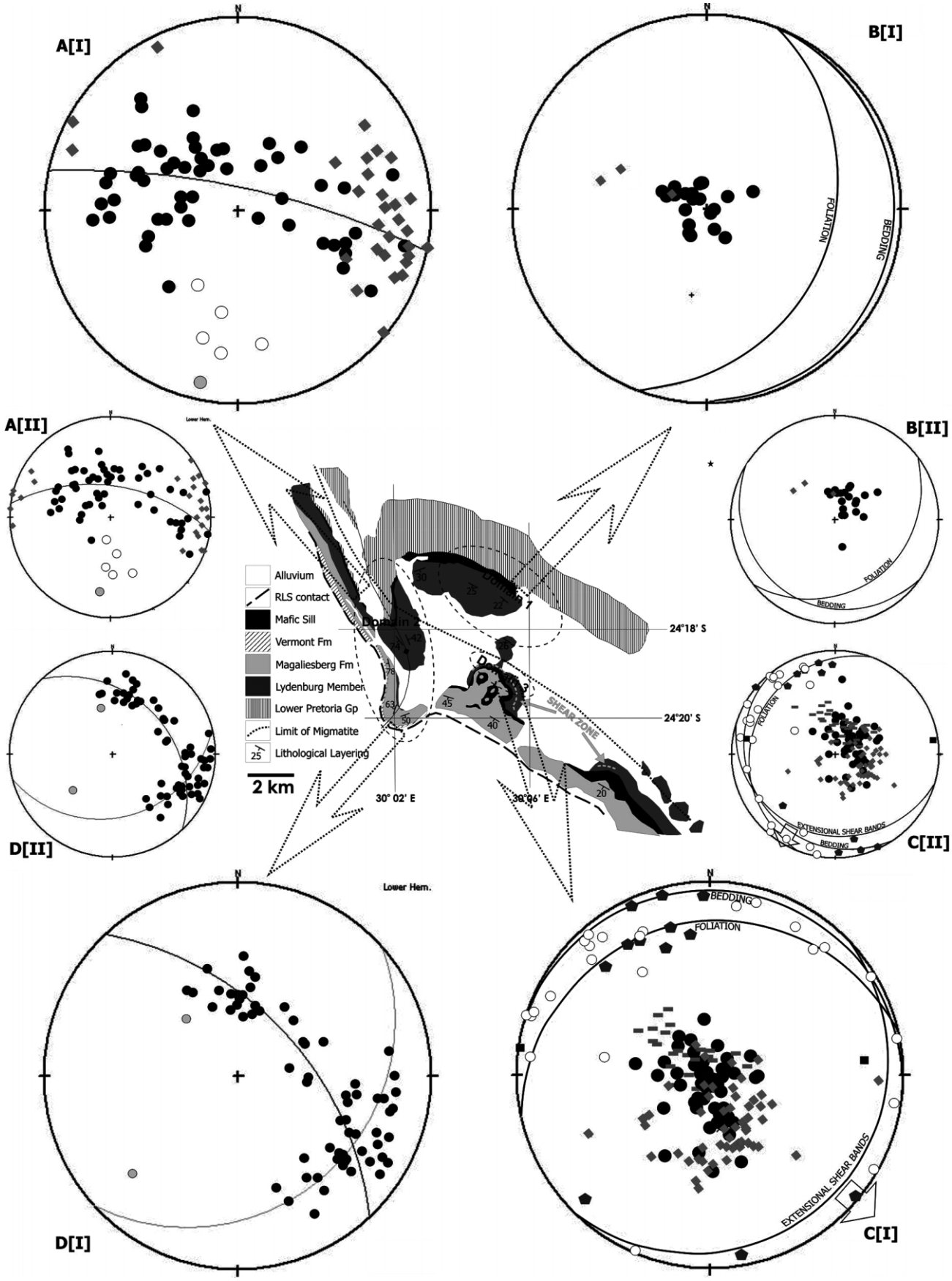

Figure 6 Geological map of the Schwerin Fold, showing stereonets for the various structural domains. Small stereonets [II]=original data. Large stereonets [I]=original data rotated 20° about a horizontal axis trending 135°. A – Core of the Schwerin anticline; B – Lower-grade schists below migmatite zone; C – Shear zone east of the anticline; D – Fold hinge within the Magaliesberg Formation adjacent to the contact with the RLS. Black circles=bedding; grey diamonds=foliation; white circles=measured fold hinge lines; grey circles=fold hinge lines from π-pole girdles; grey horizontal lines=extensional shear bands; grey pentagons=lineations; black squares=boudin long axes. B and C show average orientations for foliation, bedding, and extensional shear bands. The arrow on C[I] indicates the approximate shear direction of the shear zone.

https://doi.org/10.1017/S1755691009016119 Published online by Cambridge University Press

approximately horizontal bedding dip, and a fabric which dips shallowly away from the Schwerin Fold (Fig. 6B[I]), as expected from the fanning cleavage model (Uken & Watkeys 1997).

5.2. Quartzites adjacent to the RLS contact

The scatter of bedding data from the northwestern limb of the fold in the quartzites adjacent to the contact with the RLS may be due to broad curvature of this limb of the fold (Fig. 3), or to smaller, m-scale folding observed rarely on this limb. A m-scale open fold located on the northwestern limb may reflect this. It has a hinge orientation of 78° on 337° (Fig. 6D), which is similar to the pole to the best-fit π-pole girdle through the bedding data of 52° on 346°. This suggests that the small-scale folding of these quartzites is a consequence of broad-scale warping of the northwestern limb. Rotation of the data does not significantly affect the geometry of this domain, but does result in a shallower plunge for the fold axis in this domain.

5.3. Metasediments from the core of the Schwerin Fold

Bedding data from the Lydenburg Shale Member show more scatter than data from the quartzites adjacent to the contact with the RLS, because bedding in this domain is rotated by dm- to m-scale folds, and chaotic deformation has occurred, probably reflecting melt-assisted strain localisation. Additionally, the variability in the orientation of the fibrolitic foliation is probably due to disruption by melt-assisted strain localisation. On a broad scale, the subvertical fabric present in the core of the Schwerin Fold rotates to the more general shallowly-dipping fabric orientation, subparallel to bedding, that is present throughout the lower-grade parts of the RLS aureole (Uken 1998; Fig. 9). It is interesting to note that, whilst the present geometry of the Schwerin Fold is asymmetric, with steeper dips on the northwestern limb and shallower dips on the southeastern limb, rotation of the data to remove post-RLS tilting creates a more symmetric fold, with dips on the northwestern limb similar to those on the southeastern limb (Fig. 6A). Such symmetry would be more consistent with diapir development.

5.4. Shear Zone

The shallow E or W plunge of boudins from the shear zone (Fig. 6C) is consistent with a broadly N–S extension direction, and this does not change significantly following the rotation of the data. Lineation data also remain largely unaffected by the rotation, and the single outlier in lineation measurements (30° on 225°) coincides with the bedding-cleavage intersection orientation. There is no geographic control on the variability of fold axis orientations, and so plotting a π-pole girdle through these data would be meaningless. One possibility is that leucosome veins could have facilitated disruption and shearing-induced rotation of a set of SSE-verging folds (see below).

Apart from the folds, the orientation of structures in the shear zone indicates vergence towards the south prior to rotation. This orientation is subparallel to the axial trace in the core of the Schwerin Fold, and does not appear to be consistent with gravity-induced shedding of material off the flanks of a rising fold, which should be perpendicular to the axis of the fold. The high strains indicate substantial flattening normal to the RLS contact and subhorizontal extension. However, the ESBs and leucosome-filled shears are not conjugate, but verge asymmetrically to the south and, together with the overall fold asymmetry, indicate a significant non-coaxial strain component.

Following back-rotation to correct for the RLS dip, the vergence of the shear zone is towards the southeast (SE-dipping ESBs, NW-dipping axial planar foliation – Fig. 6C[I]). This is somewhat more compatible with gravity-induced shedding of material from a rising Schwerin Fold with a SW-trending axis, which is the axial trace of the Schwerin Fold at the contact with the RLS, even following rotation. The sense of shear for this shear zone (verging top-to-the-SE, away from the core of the fold) is the opposite of that expected for typical fold formation via a flexural slip or flexural flow mechanism, where shear sense would be expected to be reverse and top-to-the-NW towards the fold axis. However, diapirism of the floor rocks and slumping of material from the limb of the rising diapir is consistent with the vergences observed.

6. Structural relationships of the leucosomes

The leucosomes within the migmatite zone show abundant evidence of representing crystallised anatectic melts (e.g., Johnson *et al.* 2003). They are found in a wide variety of structural settings that indicate an intimate timing relationship between deformation and melting. These structural relationships vary according to structural context within the larger Schwerin Fold and shear zone.

Within the core of the pericline, leucosomes occur in en-echelon tension gashes, as discordant pods, or as diktyonitic interconnected networks (see also Johnson *et al.* 2003) between leucocratic bedding layers. Leucosomes intrude sites of localised high strain, where the bedding and foliation are displaced, truncated and rotated (Fig. 7B). Elsewhere, they occur subparallel to the subvertical foliation (Fig. 7A), as well as subparallel to bedding, but they may also be discordant to both bedding and foliation. Leucosome veins that are subparallel to the bedding and the foliation may form a network connecting these two planes. Elsewhere, smaller shear planes with 0·5–1 cm-wide leucosomes displace and rotate bedding.

In the shear zone to the southeast of the anticlinal core, leucosome orientations are generally subhorizontal, contrasting with the predominantly subvertical orientation of leucosomes in the core of the Schwerin Fold. Leucosomes are found subparallel to bedding and foliation, and locally pool below more competent psammitic layers (Fig. 7C). They truncate fold hinges along the axial planar fabric, and fill the cores of cm- to dm-scale folds (Fig. 7D). They commonly appear to have intruded preferentially along extensional shear bands (Fig. 5D). Locally, they contain disrupted schlieren of biotite (Fig. 5E) caught up during leucosome movement, that typically display geometries similar to mica 'fish', indicating movement on ESBs with a vergence towards the southeast (SSW prior to rotation). Leucosomes are also locally ptygmatically folded on a cm-scale, and develop in rare boudin necks.

7. Interpretation of the structural relationships of the leucosomes

In the core of the Schwein Fold the rocks are dominated by a subvertical axial planar fabric and upright, moderately plunging m-scale folds. Leucosomes occur in en-echelon tension gashes and evidence also exists for melt movement having occurred along the subvertical fibrolite seams (Figs 4D–E, 7B). These features are consistent with melt having been lost upwards along the steep axial planar fabric and bedding in the fold limbs, with only limited entrapment in a few extensional sites.

In the shear zone, most structures are much less steep than in the antiform. A number of syn-shearing extensional sites

https://doi.org/10.1017/S1755691009016119 Published online by Cambridge University Press

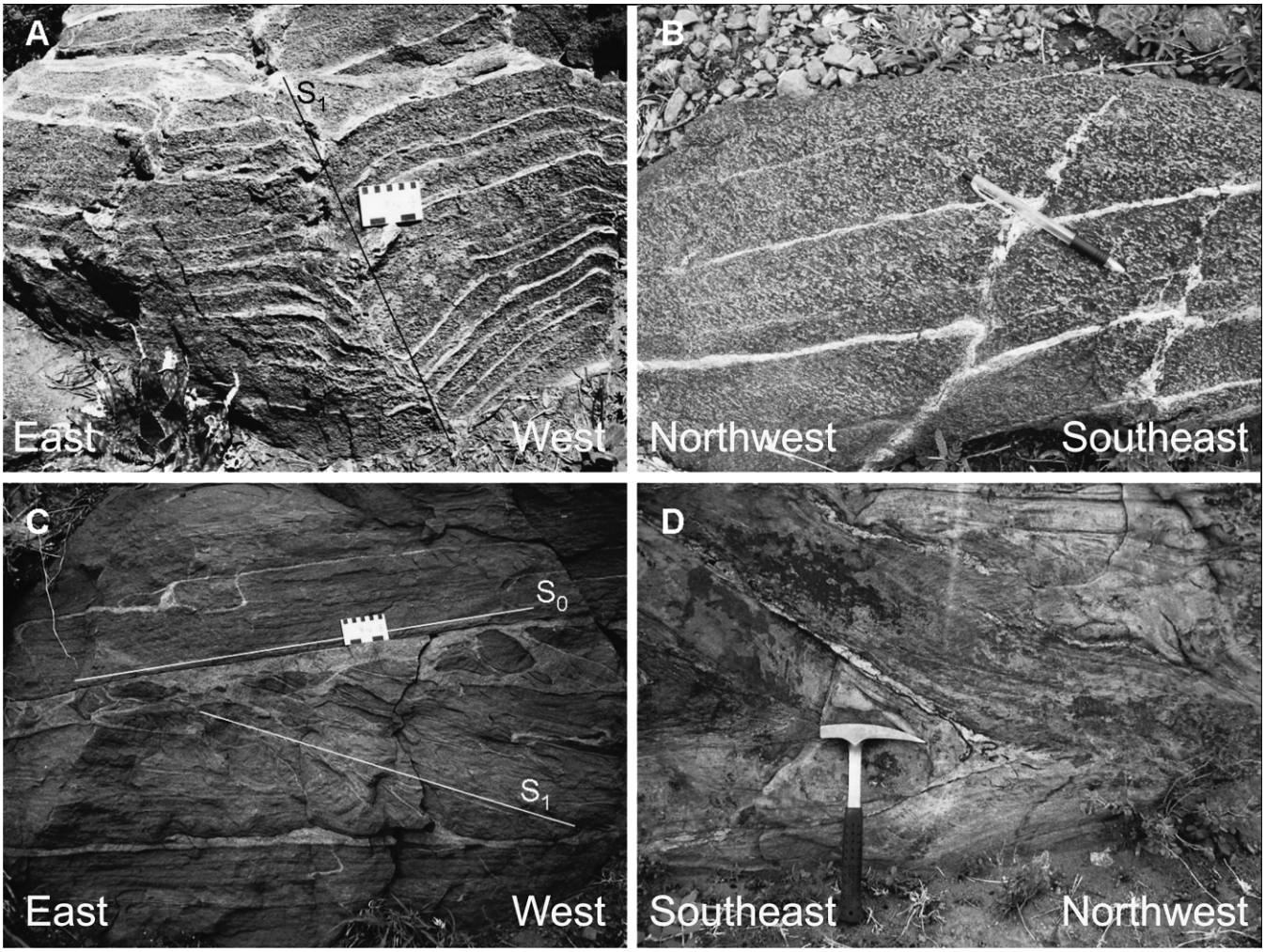

Figure 7 Leucosome structural sites: (A) Subvertical axial planar cleavage with leucosome from the migmatite zone in the core of the anticline; (B) Leucosomes within shear planes displacing lithological layering in the core of the anticline. Pencil parallel to axial planar foliation defined by fibrolite and aligned andalusite; (C) Leucosomes aligned along the NW dipping foliation in the shear zone, and along bedding; (D) Leucosome-filled dilational areas in the hinge zone of a recumbent fold in the shear zone.

(fold hinges, ESBs, boudin necks) were exploited by the melt. Additionally, the shear zone is overlain by a thick, competent quartzite layer, which may have acted as a trap for upward-migrating melts. This, in turn, would have enhanced ductility, concentrating shear strain further and possibly explaining the variable fold orientations as isolated hinges were able to rotate along slip surfaces lubricated by melt.

8. Modelling of the Bushveld Complex thermal aureole

Gerya *et al*. (2003, 2004) numerically modelled diapir development in the floor rocks beneath the RLS in two dimensions, based on the three-dimensional conceptual model of Uken & Watkeys (1997). This two-dimensional model assumes a 200–300 kg/m^3 density contrast between the dense mafic magmas of the RLS and the underlying sedimentary Pretoria Group. The rheological properties and relationships of the model depend on composition, temperature, pressure, strain rate and degree of melting and, hence, resemble the physical properties of the rocks quite well. This is evident in the sensitivity of the model to changes in the initial properties of the rocks (temperature of the floor rocks and RLS, rheological strength, lateral box size, and amplitude of the initial pericline from which these structures nucleate). A timeframe of ~800,000 years was estimated for diapir growth, and a corresponding growth rate of 8 mm/year for the most well-developed diapirs (e.g. the Phepane Dome; Fig. 1) was calculated based on the amplitude of the diapirs and the maximum timeframe for growth. The results of this modelling are considered to be robust, accurate estimates, which correspond well to the initial estimates of an ~6 mm/year growth rate made by Uken & Watkeys (1997). Since field evidence does not indicate any diapir-related structural overprint of the leucosomes in the Schwerin Fold, and there is no evidence that the lower limit of migmatite development has been significantly folded by the Schwerin Fold (isograds cut lithological boundaries and are essentially parallel to the RLS contact; Fig. 3), it can be assumed that migmatite development should have occurred over at least a similar timeframe to diapir growth. However, previous thermal modelling for the heating of the Bushveld Complex aureole using a simple one-dimensional conductive cooling approach, where the RLS is intruded as a single sill into the sediments of the Pretoria Group at ~3 km depth with a temperature of 1200–1300°C (Johnson *et al*. 2003; Harris *et al*. 2003), does not indicate such a lengthy timeframe for migmatite development. The model of Harris *et al*. (2003), in fact, assumed a RLS sill thickness of only 1500 m, and the model does not simulate temperatures sufficient to account for the melting in the aureole if conductive heating occurred. Instead, they suggested extensive fluid circulation could have accelerated the heating rate and, thus, maintained suprasolidus temperatures over significant

https://doi.org/10.1017/S1755691009016119 Published online by Cambridge University Press

Table 1 Parameters used for the multiple intrusion thermal modelling using Thermos 2·0 (© 1996 Raven Applications).

Geothermal Gradient	30°C/km
Model Depth	20 km
Cell Dimension	100 m (2000 cells)
Time Interval	1 year
Depth of Initial Intrusion	3 km
$T_{intrusion}$	1160°C to 1300°C
Time for Emplacement	75,000 years
Thermal Conductivity	6×10^{-3} cal/deg/cm^2

distances from the contact. Johnson *et al.* (2003) assumed a more realistic 7 km thickness for the RLS, and their model simulated temperatures above the solidus at orthogonal distances of >350 m from the contact. However, this model suggested that, at these distances from the contact, supra-solidus temperatures would be maintained for only ~350,000 years. Consequently, the heating model of Johnson *et al.* (2003) would require a growth rate of over 12 mm/year for the Schwerin Fold. This growth rate is double that of the initial estimates made by Uken & Watkeys (1997), and 50% greater than that calculated by Gerya *et al.* (2003).

In response to this divergence between the results from the thermal and rheological modelling the present authors have developed a thermal model of the aureole based on the intrusion of the RLS magmas in multiple pulses, rather than as a single event. This model follows Cawthorn & Walraven (1998) who developed an intrusive–crystallisation sequence based on trace element compositions and isotopic ratios of the RLS, and calculations of the amount of magma required to form the layered chromitite bands in the RLS. Their model suggests that the RLS sill was progressively inflated during distinct periods of magma addition interspersed with periods dominated by fractionation (Cawthorn & Walraven 1998).

8.1. Model setup

The thermal model was set up using similar parameters to Cawthorn & Walraven (1998) (see Table 1). The modelling was performed using the program Thermos 2·0 (© 1996 Raven Applications). Cell dimensions and time intervals were optimised to give the maximum resolution capable by the program. The total emplacement time is based on the calculations of Cawthorn and Walraven (1998).

8.2. Model results

A revised heating history for the RLS aureole has been derived using this setup. These results predict that anatexis would have extended to an orthogonal distance of >500 m from the contact and that, at a distance of 300 m from the contact, anatexis would have persisted until at least 600,000 years after intrusion. Anatexis would have continued for more than 500,000 years at a distance of ~400 m from the RLS contact (Fig. 8). This incremental intrusion model predicts higher temperatures over longer timeframes than the thermal effects of a single intrusion, and this increase in the calculated width of the migmatite zone is more compatible with the observed extent of anatexis in the aureole (>500 m, Fig. 3; although the lower limit of anatexis does vary somewhat along strike). More significantly, however, the calculated timeframe for melt generation more closely approximates the rheological modelling results for diapiric fold formation obtained by Gerya *et al.* (2003, 2004).

9. Discussion

Deformation is well known as a key factor in creating mechanisms and pathways by which buoyant anatectic melt can segregate from its source rocks and escape upwards in orogenic terrains (e.g. Brown 1994; Kisters *et al.* 1998). The Schwerin Fold region shows that similar relationships can also apply in a contact metamorphic environment. The leucosome geometries in the migmatites from the Schwerin Fold core and the area to the southeast suggest that highly variable local stresses were an important controlling factor in the movement and emplacement of granitic melts beneath the Bushveld Complex intrusion.

Both in the anticlinal core of the Schwerin Fold, as well as in the shear zone, leucosome distribution is structurally controlled. In the anticlinal core, en-echelon tension gashes provided low pressure sites where leucosome accumulated. However, the subvertical axial planar foliation and upright folds characteristic of the core of anticline provided pathways for leucosome to migrate upwards. The limited preservation of leucosomes in these features (apart from the tension gashes, only the melt escape pathways are preserved as fibrolite seams) suggests very effective melt migration once it entered these structures. This is perhaps not surprising, as the thermal gradient in the aureole is inverted, so that melts migrating upwards were actually entering hotter rocks. In the shear zone to the east of the Schwerin Fold, leucosomes are clearly located in dilational structural features such as boudin necks and ESBs that formed during subhorizontal shearing. The generally subhorizontal nature of the lithological layering and structural fabrics in this area has resulted in pooling of leucosome below more competent lithologies, with only limited upwards migration possible along the shallowly-dipping axial planar foliation in the shear zone. This concentration of leucosome in the shear zone would have increased ductility, thus concentrating further deformation in the shear zone.

It is clear from Figure 9 that the stress pattern in and around the Schwerin Fold during Bushveld metamorphism was highly variable and cannot be readily explained by a simple NW–SE compression mechanism as proposed by, e.g., Sharpe & Chadwick (1982). The leucosomes provide evidence that subvertical and subhorizontal foliations were developing simultaneously in different parts of the structure, and the foliation in the subsolidus part of the aureole displays similar syn-peak timing to the other structures but has a significantly different orientation (shallow dip obliquely away from the RLS contact). Uken & Watkeys (1997) noted similar complex fabric relationships in and around the Katkloof Fold (Fig. 1), with a subvertical axial planar fabric in the fold core rotating outwards to shallower dips until, in the interdomal areas, it is approximately bedding-parallel. These interdomal areas contain extensional features, such as boudins and conjugate ESBs, that are indicative of predominantly vertical compression and horizontal extension via pure shear (Uken 1998). In contrast, the core of the Katkloof Fold contains a variety of constrictional fold and mullion structures in addition to the subvertical foliation. Such observations suggest that fold development was driven by buoyancy, rather than regional compression.

Uken & Watkeys (1997) proposed that the diapiric folds nucleated in the necks between NE-trending finger-like intrusions of the RLS. More recently, Clarke *et al.* (2009) have demonstrated the link between aureole structures and intrusion geometry on a smaller scale around Burgersfort (Fig. 1). They attributed the strain heterogeneity in the aureole rocks to the twin causes of the stepped nature of the intrusive contact, which locally cuts across the Pretoria Group stratigraphy, and subsequent magmatic inflation of the individual fingers of

https://doi.org/10.1017/S1755691009016119 Published online by Cambridge University Press

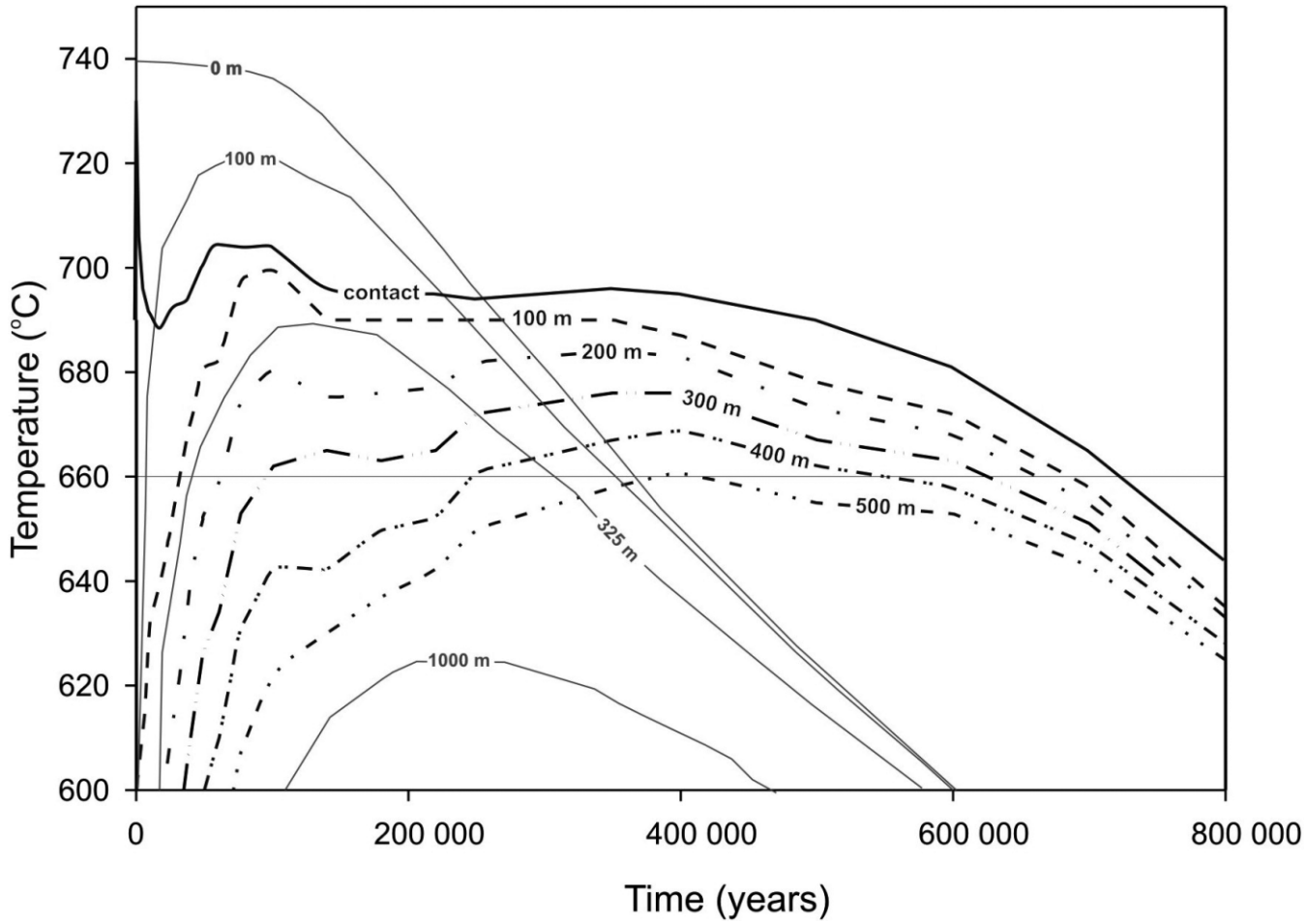

Figure 8 Results of thermal modelling of the RLS aureole, using the single intrusion model of Johnson *et al.* (2003) (grey lines), and the multiple intrusion model of Cawthorn & Walraven (1998) (black lines). Note that for the single intrusion model peak temperatures are higher and are achieved earlier, but cool below the solidus quicker (<400,000 years after the intrusion of the RLS). In the case of the multiple intrusion model the solidus is exceeded further from the contact and, at 300 m from the contact, suprasolidus temperatures are maintained for ~600,000 years. Irregularities in the curves are due to the periodic emplacement of magma into the RLS chamber, as described in Cawthorn & Walraven (1998).

the RLS sheet intrusion. Where the intrusion fingers were separated by country rock, or where a step occurred, lateral inflation induced compressional stresses in the country rock, generating symmetric or asymmetric structures depending on the exact intrusion geometry. A local stress regime induced by the geometry of the intrusion can more readily explain such features as the curvature of the Schwerin Fold axial trace and the restricted extent of the shear zone orthogonal to the Schwerin Fold axis. It could also explain the subsolidus foliation in the northeastern part of the study area, which dips obliquely away from, rather than towards, the main RLS contact. If Clarke *et al*'s (2009) model is applied, this foliation was induced by a (now-eroded) transgressive RLS contact dipping southeast and lying southeast of the study area. The exact timing of development of this lower-grade foliation relative to the axial planar and shear foliations is a matter of debate. Figure 8 shows that the metamorphic peak is attained progressively later in rocks further from the RLS contact; however, it is likely that peak conditions were reached before termination of deformation related to the formation of the fold. The fact that the andalusite, cordierite and garnet porphyroblasts in the lower-grade rocks show a late- to post-kinematic timing relative to this foliation (compared with the pre- to syn-kinematic relationships in both the fold and the shear zone), may reflect the delayed thermal response in the lower aureole compared with the rapid transfer of stresses that would ultimately have driven foliation development once appropriate metamorphic conditions were reached.

The Schwerin Fold is, thus far, the only periclinal structure in the Bushveld Complex aureole that appears to be associated with a large shear zone. As shown in the diagrammatic representation of the structures in the Schwerin Fold (Fig. 9), the development of the shear zone to the east of the pericline is compatible with slumping of ductile material from the flanks of a rising diapir. This is supported by the restricted areal distribution of the shear zone, which disappears towards the southeast away from the fold. Similar slumping effects have been noted by Clarke *et al.* (2005) adjacent to the Steelpoort Pericline, but only in magmatic RLS rocks. The western limb of the Schwerin Fold appears to be extremely attenuated (Fig. 3) but contains no evidence of shearing, although outcrop of non-quartzitic rocks is poor. If the Schwerin shear zone is unique, the reason may lie in the proximity of the thick quartzite unit of the Magaliesberg Formation to the RLS contact in the Schwerin area. This unit may have acted both as a barrier to rising anatectic melts and as a coherent structural unit which then slid southeastwards off the diapirically rising Schwerin pericline, thus focusing shear stresses in the melt-weakened unit immediately below it. In other periclines, the RLS contact cuts across more-finely-bedded, less refractory, lithologies which would have undergone general melt-induced weakening that, together with their original rheological

https://doi.org/10.1017/S1755691009016119 Published online by Cambridge University Press

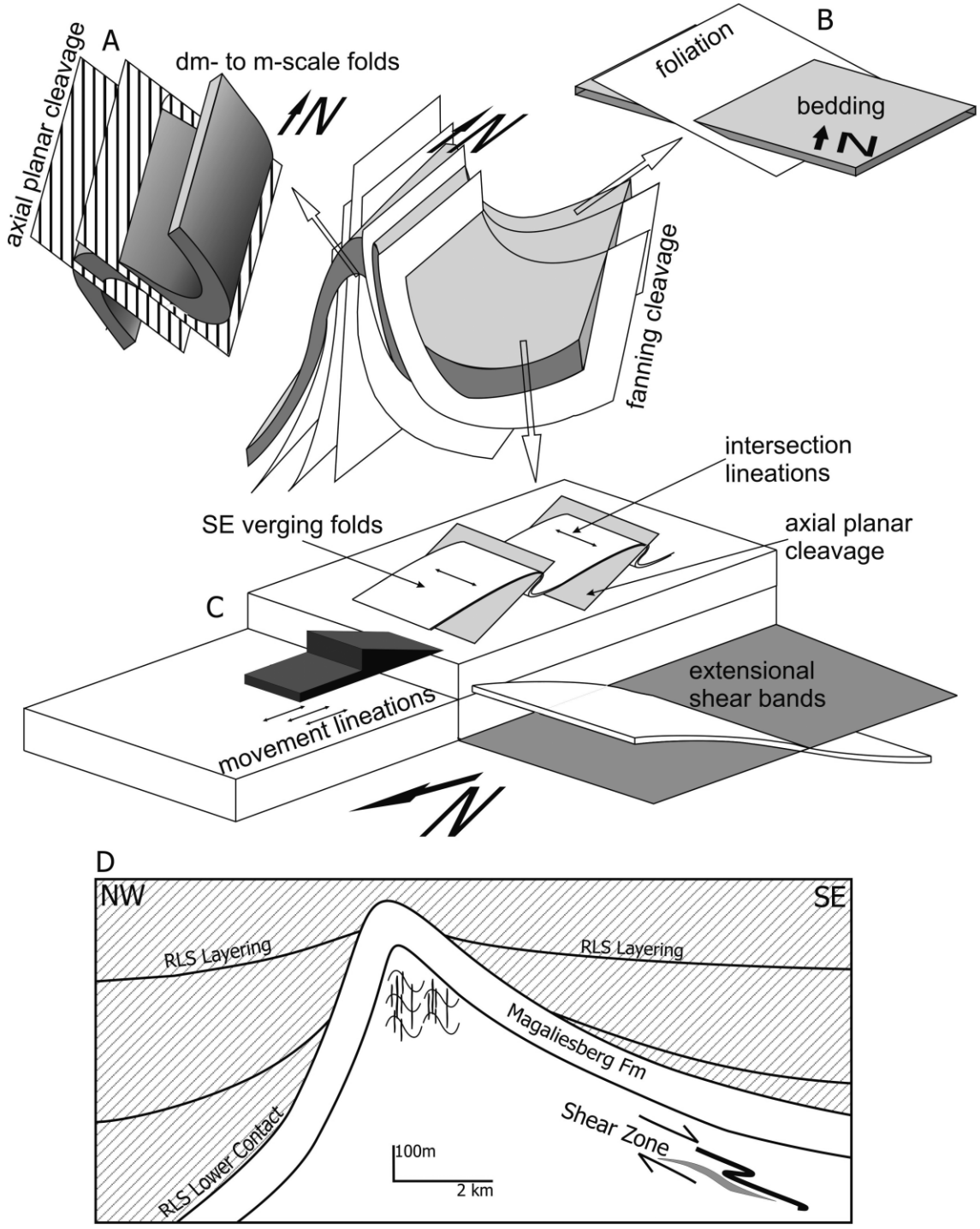

Figure 9 Diagrammatic summary of the structural features found within the study area: (A) The NE domain furthest from the RLS contains a weak ESE-dipping foliation and subhorizontal bedding; (B) The core of the anticline contains dm- to m-scale folds and a subvertical axial planar cleavage; (C) The shear zone contains SE-verging, tight to isoclinal folds with an axial planar cleavage. Bedding-cleavage intersection lineations and movement (mineral extension) lineations are present on bedding surfaces. ESBs have a SE vergence. Bedding is subhorizontal (following restoration by rotation – see Fig. 6); (D) Schematic representation of the Schwerin Fold showing subvertical leucosomes oriented axial planar to folds in the core of the pericline, with the top-to-the-SE shear zone resulting from gravitational slumping of material off the eastern limb of the fold, and RLS layering truncated and folded by the diapiric fold.

properties, would have distributed the limb shear stresses more homogeneously.

Another question which arises from the Schwerin Fold is whether the leucosome present in the migmatites contributed to the overall buoyancy of the fold, and accelerated the diapiric rise of the floor rocks. Johnson *et al.* (2003) noted that Marginal Zone norites of the RLS are brecciated and invaded by significant quantities of leucosome near the Derde Gelid Pericline south of the study area (Fig. 1). A similar concentration of leucosomes is not seen in the quartzites or RLS in the hinge of the Schwerin Fold, but the efficiency of melt segregation and migration attested to by the fibrolite seams in the core of the fold makes it most likely that such an accumulation did form in the now-eroded crest of the fold. Notwithstanding this, when a buoyant melt is created and segregated from its source rock, a denser residue/restite is

https://doi.org/10.1017/S1755691009016119 Published online by Cambridge University Press

left behind. In this case, the overall density of the rock volume does not change, as the buoyancy of the magma is counteracted by the increased density of the restite. Field relations indicate that the Schwerin Fold encompasses the entire volume of suprasolidus rock and, thus, that no significant buoyancy effect is likely to have existed due to melt extraction. Furthermore, Johnson *et al*. (2003) estimated that overall melting in the Schwerin Fold is unlikely to have exceeded 10 vol%. The primary impetus for diapirism must, thus, have been the density contrast (200–300 kg/m^3; Gerya *et al*. 2003) between the upper Pretoria Group floor rocks and the overlying RLS, with an irregular lower RLS contact created by the finger-like geometry of the magma intrusions (Uken & Watkeys 1997; Clarke *et al*. 2009).

The interrelationship between the thermal and deformation effects in the upper contact aureole caused by the intrusion of the RLS must be evaluated within the context of a model that acknowledges the multi-stage nature of inflation of the Bushveld magma chamber (Cawthorn & Walraven 1998). In contrast to the single-stage intrusion models (e.g., Johnson *et al*. 2003; Harris *et al*. 2003), which would require doming rates double that calculated by Gerya *et al*. (2003), the multiple-intrusion model generates slightly lower peak temperatures but a longer-lived metamorphic effect that achieves very good agreement with the timescale for diapiric fold development deduced by Gerya *et al*. (2003).

10. Conclusions

The segregation and migration of melt in the contact aureole beneath the RLS is intimately linked to the structural development of the aureole, particularly in areas such as the Schwerin Fold, where structures are more pronounced, and where deformation is clearly contemporaneous with metamorphism and migmatisation within the aureole. Of additional importance is the absolute timing of metamorphism, migmatisation and diapir development in the contact aureole. The Schwerin Fold developed over ~600 000 years, with a growth rate of ~8 mm/year, which is consistent with modelled estimates for the duration of diapir development elsewhere in the aureole (Gerya *et al*. 2003). A simple, one-dimensional, cooling model of a 7–8 km-thick sill does not account for this – rather, a model of multiple intrusive pulses for the RLS is more consistent with the longer duration of diapir development. It is evident that migration and accumulation of buoyant leucosome is controlled by the structural geometry of the area in which migmatisation is occurring – subvertical structures allow these leucosomes to escape upwards, whilst subhorizontal structures result in the accumulation of leucosome, in turn triggering a local increase in ductility. The latter may well have led to slumping along the diapir flank being localised in a broad extensional shear zone.

11. Acknowledgements

We are grateful to Anglo Platinum for logistical support during field work for this study. Tim Johnson and Chris Gerbi are thanked for constructive reviews which improved the quality of the manuscript.

12. References

Bai, Q., Jin, Z.-M. & Green II, W. 1997. Experimental investigation of the rheology of partially molten peridotite at upper mantle pressures and temperatures. *In* Holness, M. B. (ed.) *Deformation-enhanced Fluid Transport in the Earth's Crust and Mantle*, 40–61. *The Mineralogical Society Series* **8**. London: Chapman & Hall.

Bhadra, S., Das, S. & Bhattacharya, A. 2007. Shear Zone-hosted Migmatites (Eastern India): the Role of Dynamic Melting in the Generation of REE-depleted Felsic Melts, and Implications for Disequilibrium Melting. *Journal of Petrology* **48**, 435–57.

Brown, M. 1994. The generation, segregation, ascent and emplacement of granite magma: the migmatite-to-crustally-derived granite connection in thickened orogens. *Earth Science Reviews* **36**, 83–130.

Brown, M. 2005. Synergistic effects of melting and deformation: an example from the Variscan belt, western France. *In* Gapais, D., Brun, J. P. & Cobbold, P. R. (eds) *Deformation Mechanisms, Rheology and Tectonics: from minerals to the Lithosphere*, 205–26. *Geological Society, London, Special Publication* **243.** Bath, UK: The Geological Society Publishing House.

Brown, M., Averkin, Y. A., McLellan, E. L. & Sawyer, E. W. 1995. Melt segregation in migmatites. *Journal of Geophysical Research* **100**, 15655–79.

Brown, M. & Solar, G. S. 1998. Shear zone systems and melts: feedback relations and self-organization in orogenic belts. *Journal of Structural Geology* **20**, 211–27.

Button, A. 1978. Diapiric structures in the Bushveld, north-eastern Transvaal. *Information Circular, Economic Geology Research Unit* **96.** Johannesburg, South Africa: University of the Witwatersrand. 13 pp.

Cawthorn, R. G. & Walraven, F. 1998. Emplacement and crystallization time for the Bushveld Complex. *Journal of Petrology* **39**, 1669–87.

Clarke, B. M., Uken, R., Watkeys, M. K. & Reinhardt, J. 2005. Folding of the Rustenburg Layered Suite adjacent to the Steelpoort pericline: implications for syn-Bushveld tectonism in the eastern Bushveld Complex. *South African Journal of Geology* **108**, 397–412.

Clarke, B. M., Uken, R. & Reinhardt, J. 2009. The geometry and emplacement mechanics of a Bushveld Complex peridotite body. *South African Journal of Geology* **112**, 141–62.

Eriksson, P. G., Schweitzer, J. K., Bosch, P. J. A., Schereiber, U. M., Van Deventer, J. L. & Hatton, C. J. 1993. The Transvaal Sequence: an overview. *Journal of African Earth Sciences* **16**, 25–51.

Gerya, T. V., Uken, R., Reinhardt, J., Watkeys, M. K., Maresch, W. V. & Clarke, B. M. 2003. Cold fingers in hot magma: numerical modeling of country rock diapirs in the Bushveld Complex, South Africa. *Geology* **31**, 753–6.

Gerya, T. V., Uken, R., Reinhardt, J., Watkeys, M. K., Maresch, W. V. & Clarke, B. M. 2004. 'Cold' diapirs triggered by intrusion of the Bushveld Complex: Insight from two-dimensional numerical modeling. *In* Whitney, D. L., Teyssier, C. & Siddoway, C. S. (eds) *Gneiss Domes in Orogeny*, 117–27. *Geological Society of America Special Paper* **380.** Boulder, Colorado & Lawrence, Kansas: Geological Society of America & University of Kansas Press.

Gleason, G., Bruce, V. & Green, H. W. 1999. Experimental investigation of melt topology in partially molten quartzofeldspathic aggregates under hydrostatic and non-hydrostatic stress. *Journal of Metamorphic Geology* **17**, 705–22.

Hand, M. & Dirks, P. H. G. M. 1992. The influence of deformation on the formation of axial-planar leucosomes and the segregation of small melt bodies within the migmatitic Napperby Gneiss, central Australia. *Journal of Structural Geology* **14**, 591–604.

Harris, N., McMillan, A., Holness, M., Uken, R., Watkeys, M., Rogers, N. & Fallick, A. 2003. Melt generation and fluid flow in the thermal aureole of the Bushveld Complex. *Journal of Petrology* **44**, 1031–54.

Hartzer, F. J. 1995. Transvaal Supergroup inliers: geology, tectonic development and relationship with the Bushveld Complex, South Africa. *Journal of African Earth Sciences* **21**, 521–47.

Holyoke, C. W. & Rushmer, T. 2002. An experimental study of grain scale melt segregation mechanisms in two common crustal rock types. *Journal of Metamorphic Geology* **20**, 493–512.

Johnson, T. E., Gibson, R. L., Brown, M., Buick, I. S. & Cartwright, I. 2003. Partial Melting of metapelitic rocks beneath the Bushveld Complex, South Africa. *Journal of Petrology* **44**, 789–813.

Johnson, T., Brown, M., Gibson, R. & Wing, B. 2004. Spinel-cordierite symplectites replacing andalusite: evidence for melt-assisted diapirism in the Bushveld Complex, South Africa. *Journal of Metamorphic Geology* **22**, 529–45.

Kisters, A. F. M., Gibson, R. L., Charlesworth, E. G. & Anhaeusser, C. R. 1998. The role of strain localization in the segregation and ascent of anatectic melts, Namaqualand, South Africa. *Journal of Structural Geology* **20**, 229–42.

Kretz, R. 1983. Symbols for rock-forming minerals. *American Mineralogist* **68**, 277–79.

Longridge, L. 2006. *Structural and metamorphic evolution of the Schwerin Fold, northeastern Bushveld Complex, Limpopo Province.* Honours Thesis, University of the Witwatersrand, Johannesburg, South Africa. 42p.

Letts, S. A. 2007. *The palaeomagnetic significance of the Bushveld Complex and related 2 Ga magmatic rocks in ancient continental entities*. PhD Thesis, University of the Witwatersrand, Johannesburg, South Africa. 228 pp.

du Plessis, C. P. & Walraven, F. 1990. The tectonic setting of the Bushveld Complex in southern Africa, part 1. Structural deformation and distribution. *Tectonophysics* **179**, 305–19.

Rosenberg, C. L. & Berger, A. 2000. Syntectonic Melt Pathways in Granitic Gneisses, and Melt-Induced Transitions in Deformation Mechanisms. *Physics and Chemistry of the Earth* **26**, 287–93.

Sawyer, E. W. 1991. Disequilibrium melting and the rate of melt-residuum separation during migmatization of mafic rocks from the Grenville Front, Quebec. *Journal of Petrology* **32**, 701–38.

Schwellnus, J. S. I., Engelbrecht, L. N. J., Coertze, F. J., Russell, H. D., Malherbe, S. J., van Rooyen, D. P. & Cooke, R. 1962. *The geology of the Oliphants River area*. Explanation to Sheets 2429B (Chuniespoort) and 2430A (Wolkberg). Geological Survey of South Africa.

Sharpe, M. R. & Chadwick, B. 1982. Structures in Transvaal Sequence rocks within and adjacent to the eastern Bushveld Complex. *Transactions of the Geological Society of South Africa* **85**, 29–41.

Uken, R. 1998. *The Geology and Structure of the Bushveld Complex metamorphic aureole in the Olifants River area.* PhD Thesis, University of Natal, Durban, South Africa. 277 pp.

Uken, R. & Watkeys, M. K. 1997. Diapirism initiated by the Bushveld Complex, South Africa. *Geology* **25** 723–6.

Vernon, R. H., Collins, W. J. & Richards, S. W. 2003. Contrasting magmas in metapelitic and metapsammitic migmatites in the Cooma Complex, Australia. *Visual Geosciences* **8**, 1–22.

Walraven, F., Armstrong, R. A. & Kruger, F. J. 1990. A chronostratigraphic framework for the north-central Kaapvaal craton, the Bushveld Complex and Vredefort structure. *Tectonophysics* **171**, 23–48.

Waters, D. J. & Lovegrove, D. P. 2002. Assessing the extent of disequilibrium and overstepping of prograde metamorphic reactions in metapelites from the Bushveld Complex aureole, South Africa. *Journal of Metamorphic Geology* **20**, 135–49.

MS received 12 December 2007. Accepted for publication 10 June 2008 (Stellenbosch); 15 January 2009 (RSE).